Electronic Supplementary Material (ESI) for Physical Chemistry Chemical Physics.

Deactivation dynamics of cyclic ethers of variable ring size - Supplementary Information

Anja Röder[a,f], Anders B. Skov,[b], Andrey E. Boguslavskiy[a,c–f], Rune Lausten,[d] and Albert Stolow[a,c–f]

[a] *Department of Chemistry, University of Ottawa, 10 Marie Curie, Ottawa, Ontario, K1N 6N5, Canada; E-mail: aroder@uottawa.ca*

[b] *Department of Chemistry, University of Copenhagen, Universitetsparken 5, 2100 København Ø, Denmark*

[c] *Department of Physics, University of Ottawa, 150 Louis-Pasteur Pvt, Ottawa, Ontario, Canada, K1N 6N5*

[d] *National Research Council of Canada, 100 Sussex Drive, Ottawa, Ontario, K1A 0R6, Canada*

[e] *Max Planck University of Ottawa Centre for Extreme and Quantum Photonics, University of Ottawa, Ottawa, Canada*

[f] *Joint Centre for Extreme Photonics, National Research Council and University of Ottawa, Ottawa, ON, K1A 0R6, Canada*

1 Ground State Structures of neutral cyclic ethers

1.1 THP

		Coordinates (Ångstrom.)		
Atom		X	Y	Z
1	C	0.1977319637	-0.7631907625	1.1707856635
2	C	-0.2283502566	0.6939116659	1.2467135246
3	C	0.2429274786	1.4375183922	0.0000000000
4	C	-0.2283502566	0.6939116659	-1.2467135246
5	C	0.1977319637	-0.7631907625	-1.1707856635
6	O	-0.3045317141	-1.3954585806	0.0000000000
7	H	-0.1876727267	-1.3382392005	2.0112713836
8	H	1.2951230854	-0.8305252290	1.1780278966
9	H	0.1801528690	1.1467191723	2.1527869542
10	H	-1.3178146708	0.7365840404	1.3143232744
11	H	1.3366412001	1.4814470662	0.0000000000
12	H	-0.1196037120	2.4663875632	0.0000000000
13	H	0.1801528690	1.1467191723	-2.1527869542
14	H	-1.3178146708	0.7365840404	-1.3143232744
15	H	1.2951230854	-0.8305252290	-1.1780278966
16	H	-0.1876727267	-1.3382392005	-2.0112713836

Table 1: Ground state geometry of neutral THP at the MP2/aug-cc-pVTZ level in cartesian coordinates.

1.2 THF

		Coordinates (Ångstrom.)		
Atom		X	Y	Z
1	C	1.1616379728	-0.1419542130	0.4204496319
2	C	0.7244839125	0.2417214954	-0.9866337480
3	C	-0.7244839125	-0.2417214954	-0.9866337480
4	C	-1.1616379728	0.1419542130	0.4204496319
5	O	0.0000000000	0.0000000000	1.2501566303
6	H	1.9483452608	0.4964371194	0.8204152866
7	H	1.5004504436	-1.1816073071	0.4538287220
8	H	1.3392914464	-0.2199995590	-1.7570077922
9	H	0.7588857158	1.3246331375	-1.1120674481
10	H	-0.7588857158	-1.3246331375	-1.1120674481
11	H	-1.3392914464	0.2199995590	-1.7570077922
12	H	-1.9483452608	-0.4964371194	0.8204152866
13	H	-1.5004504436	1.1816073071	0.4538287220

Table 2: Ground state geometry of neutral THF at the MP2/aug-cc-pVTZ level in cartesian coordinates.

1.3 TMO

		Coordinates (Ångstrom.)		
Atom		X	Y	Z
1	C	0.0412478985	-0.0790098100	1.0279022424
2	C	-1.0612773863	0.2072672738	0.0000000000
3	O	1.0636127110	-0.0196321133	0.0000000000
4	H	-0.0124872014	-1.0774125379	1.4676421746
5	H	-1.3786149497	1.2460818668	0.0000000000
6	H	-1.9262769465	-0.4492756719	0.0000000000
7	H	-0.0124872014	-1.0774125379	-1.4676421746
8	C	0.0412478985	-0.0790098100	-1.0279022424
9	H	0.2115651478	0.6603608559	1.8084059601
10	H	0.2115651478	0.6603608559	-1.8084059601

Table 3: Ground state geometry of neutral TMO at the MP2/aug-cc-pVTZ level in cartesian coordinates.

2 Ground State Structures of cationic cyclic ethers

2.1 THP

		Coordinates (Ångstrom.)		
Atom		X	Y	Z
1	C	0.2371317147	-0.8266871975	1.1452669018
2	C	-0.2434277801	0.7458938559	1.2546577178
3	C	0.2464211489	1.4071533614	0.0000000000
4	C	-0.2434277801	0.7458938559	-1.2546577178
5	C	0.2371317147	-0.8266871975	-1.1452669018
6	O	-0.3213401604	-1.2607642665	0.0000000000
7	H	-0.2074797285	-1.3380189421	1.9947768778
8	H	1.3277019958	-0.8101954372	1.1364410255
9	H	0.2235974141	1.0939433689	2.1755015531
10	H	-1.3265435849	0.7332369728	1.3473359863
11	H	1.3293352510	1.5247546171	0.0000000000
12	H	-0.1998417594	2.4173471802	0.0000000000
13	H	0.2235974141	1.0939433689	-2.1755015531
14	H	-1.3265435849	0.7332369728	-1.3473359863
15	H	1.3277019958	-0.8101954372	-1.1364410255
16	H	-0.2074797285	-1.3380189421	-1.9947768778

Table 4: Ground state geometry of cationic THP at the MP2/aug-cc-pVTZ level in cartesian coordinates.

2.2 THF

		Coordinates (Ångstrom.)		
Atom		X	Y	Z
1	C	1.1616379728	-0.1419542130	0.4204496319
2	C	0.7244839125	0.2417214954	-0.9866337480
3	C	-0.7244839125	-0.2417214954	-0.9866337480
4	C	-1.1616379728	0.1419542130	0.4204496319
5	O	0.0000000000	0.0000000000	1.2501566303
6	H	1.9483452608	0.4964371194	0.8204152866
7	H	1.5004504436	-1.1816073071	0.4538287220
8	H	1.3392914464	-0.2199995590	-1.7570077922
9	H	0.7588857158	1.3246331375	-1.1120674481
10	H	-0.7588857158	-1.3246331375	-1.1120674481
11	H	-1.3392914464	0.2199995590	-1.7570077922
12	H	-1.9483452608	-0.4964371194	0.8204152866
13	H	-1.5004504436	1.1816073071	0.4538287220

Table 5: Ground state geometry of cationic THF at the MP2/aug-cc-pVTZ level in cartesian coordinates.

2.3 TMO

		Coordinates (Ångstrom.)		
Atom		X	Y	Z
1	C	0.0412478985	-0.0790098100	1.0279022424
2	C	-1.0612773863	0.2072672738	0.0000000000
3	O	1.0636127110	-0.0196321133	0.0000000000
4	H	-0.0124872014	-1.0774125379	1.4676421746
5	H	-1.3786149497	1.2460818668	0.0000000000
6	H	-1.9262769465	-0.4492756719	0.0000000000
7	H	-0.0124872014	-1.0774125379	-1.4676421746
8	C	0.0412478985	-0.0790098100	-1.0279022424
9	H	0.2115651478	0.6603608559	1.8084059601
10	H	0.2115651478	0.6603608559	-1.8084059601

Table 6: Ground state geometry of cationic TMO at the MP2/aug-cc-pVTZ level in cartesian coordinates.

3 Visual Comparison of neutral and cationic ground states

3.1 THP

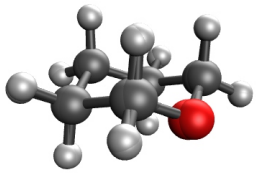

Figure 1: Overlay of neutral and cationic ground state geometries of THP.

3.2 THF

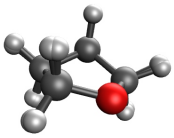

Figure 2: Overlay of neutral and cationic ground state geometries of THF.

3.3 TMO

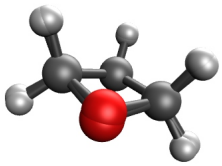

Figure 3: Overlay of neutral and cationic ground state geometries of TMO.

4 Vertical Excitation Energies calculated with ADC(2) and ADC(3)

	TMO (C_S)				THF (C_2)				THP (C_S, chair)			
	Symm	E/eV (nm)	f /10^{-4}	Character	Sym.	E/eV(nm)	f /10^{-4}	Character	Sym.	E/eV(nm)	f /10^{-4}	Character
1	2A'	5.74 (216)	92	n-Ry3s	1B	5.66 (219)	55	n-Ry3s	2A'	5.85 (212)	104	n-Ry3s
2	3A'	6.15 (202)	29	n-Ry3p_x	2A	6.17 (201)	7.6	n-Ry3p_y	3A'	6.21 (200)	310	n-Ry3p_z
3	1A"	6.24 (199)	2.1	n-Ry3p_z	3A	6.31 (197)	1.6	n-Ry3p_z	1A"	6.33 (196)	245	n-Ry3p_x
4	4A'	6.33 (196)	156	n-Ry3p_y	2B	6.46 (192)	9.9	n-Ry3p_x	4A'	6.43 (193)	15	n-Ry3p_y
5	5A'	7.13 (174)	105	n-Ry3d_{z^2}	3B	6.95 (178)	103	n-Ry3d_{z^2}	5A'	6.97 (178)	6.8	n-Ry3$d_{x^2-y^2}$
6	2A"	7.32 (169)	340	n-Ry3d_{xz}	4A	7.09 (175)	3.7	n-Ry3d_{xz}	2A"	7.05 (176)	13	n-Ry3d_{xy}
7	6A'	7.53 (165)	15	n-Ry3d_{xy}	4B	7.12 (174)	436	n-Ry3d_{yz}	3A"	7.12 (174)	22	n-Ry3d_{xz}
8	7A'	7.59 (163)	216	σ_x-Ry3s	5B	7.29 (170)	60	n-Ry3d_{xy}	6A'	7.16 (173)	21	n-Ry3d_{z^2}
9	3A"	7.65 (162)	0.21	n-Ry3d_{xy}	5A	7.42 (167)	6.6	n-Ry3$d_{x^2-y^2}$	7A'	7.31 (170)	52	n-Ry3d_{yz}

Table 7: The symmetries, vertical excitation energies E and oscillator strengths f of first nine excited states of TMO, THF and THP calculated at the ADC(2)/aug-cc-pVDZ level of theory.

	TMO (C_S)				THF (C_2)				THP (C_S, chair)			
	Sym.	E/eV (nm)	$f/10^{-4}$	Character	Sym.	E/eV (nm)	$f/10^{-4}$	Character	Sym.	E/eV (nm)	$f/10^{-4}$	Character
1	2A'	7.00 (177)	59	n-Ry3s	1B	6.96 (178)	97	n-Ry3s	2A'	7.12 (174)	79	n-Ry3s
2	3A'	7.31 (169)	120	n-Ry3p_x	2A	7.55 (164)	0.17	n-Ry3p_y	3A'	7.48 (166)	460	n-Ry3p_z
3	1A"	7.56 (164)	2.2	n-Ry3p_z	3A	7.68 (161)	3.4	n-Ry3p_z	1A"	7.66 (162)	340	n-Ry3p_x
4	4A'	7.71 (160)	210	n-Ry3p_y	2B	7.79 (159)	22	n-Ry3p_x	4A'	7.70 (161)	12	n-Ry3p_z
5	5A'	8.44 (147)	130	n-Ry3d_{z^2}	3B	8.16 (152)	170	n-Ry3d_{z^2}	5A'	8.16 (152)	9.4	n-Ry3$d_{x^2-y^2}$
6	6A'	8.70 (142)	270	σ_x-Ry3s	4A	8.50 (145)	2.6	n-Ry3d_{xz}	2A"	8.37 (148)	5.5	n-Ry3d_{xy}
7	2A"	8.76 (141)	6.70	n-Ry3d_{xz}	4B	8.52 (145)	640	n-Ry3d_{yz}	6A'	8.43 (147)	69	n-Ry3d_{z^2}
8	3A"	8.84 (140)	4.7	σ_y-Ry3s	5B	8.63 (143)	71	n-Ry3d_{xy}	3A"	8.46 (148)	25	n-Ry3d_{xz}
9	7A'	8.89 (139)	15	n-Ry3d_{xy}	5A	8.74 (142)	38	σ-Ry3s	7A'	8.53 (145)	68	σ^*-Ry3s

Table 8: The symmetries, vertical excitation energies E and oscillator strengths f of first nine excited states of TMO, THF and THP calculated at the ADC(3)/aug-cc-pVDZ level of theory.

5 NTOs at elongated bond lengths

5.1 THP

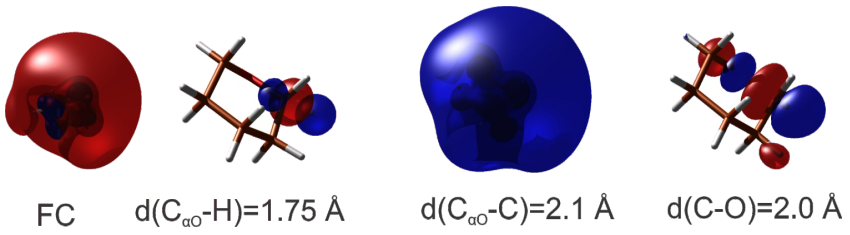

Figure 4: NTOs of S_1 of THP at the Franck-Condon region and several selected bond elongations.

5.2 THF

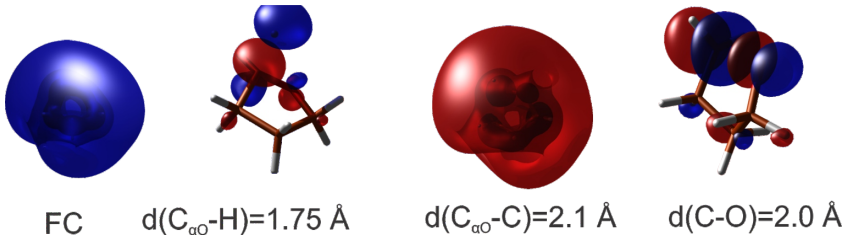

Figure 5: NTOs of S_1 of THF at the Franck-Condon region and several selected bond elongations.

5.3 TMO

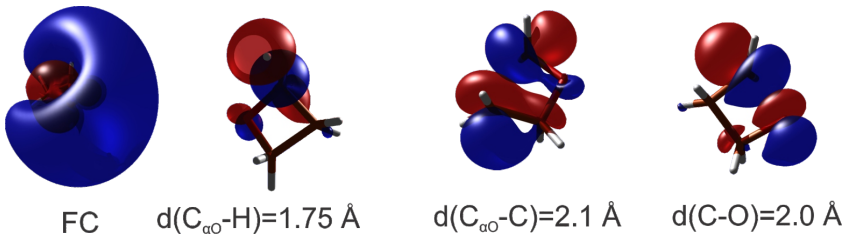

Figure 6: NTOs of S_1 of TMO at the Franck-Condon region and several selected bond elongations.

6 Raw VMI images at selected times

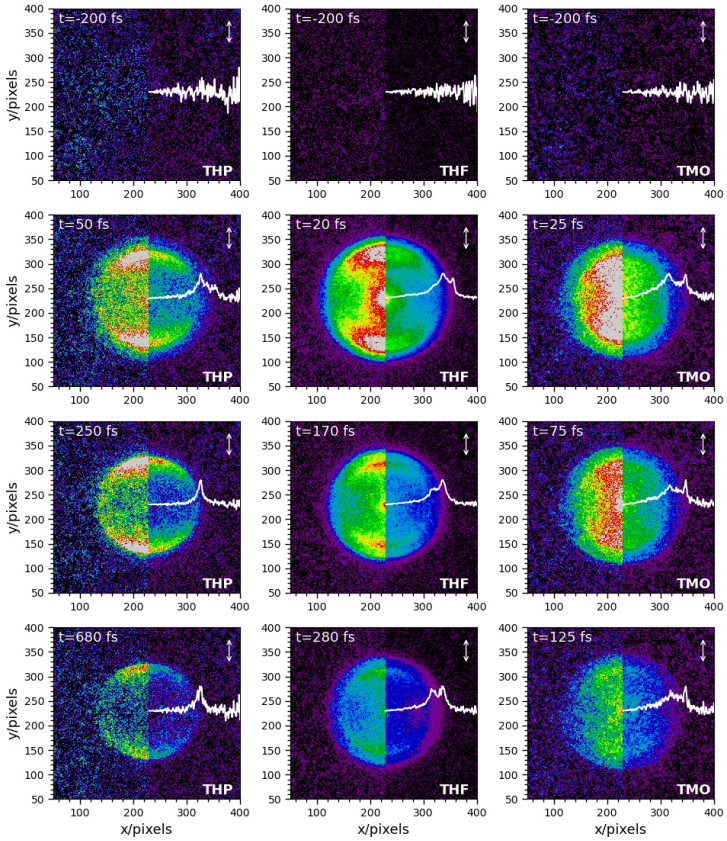

Figure 7: Rotated raw VMI-images at selected times for THP (first column), THF (second column) and TMO (third column). The images of each series are normalized on the first image, and background of pump/probe only has been subtracted. The intensity of the left side of each image has been multiplied by 2 in order to highlight weak features. The white line corresponds to the inverted radial integration.

7 TRPES at higher kinetic energies

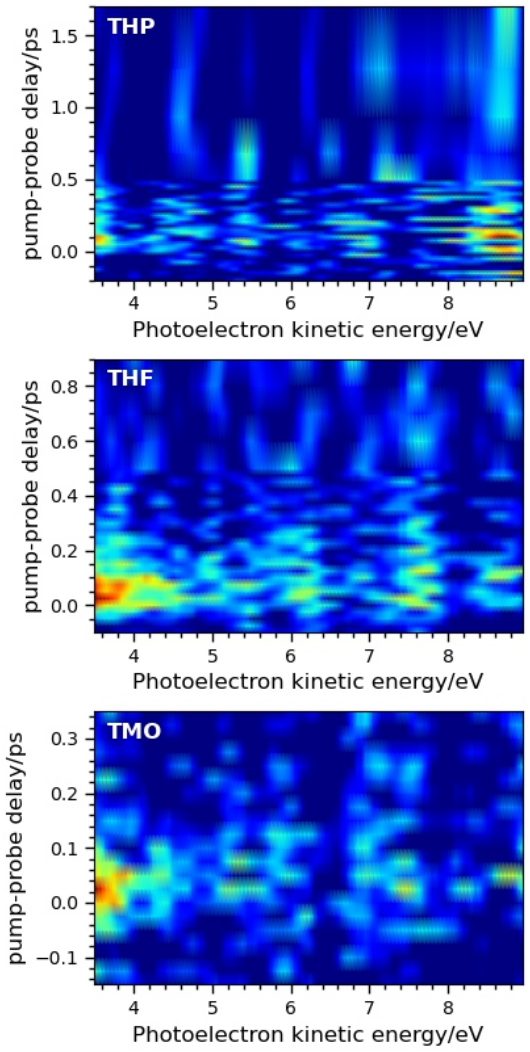

Figure 8: Time-resolved photoelectron spectra for THP (top), THF (middle) and TMO (bottom) at higher kinetic energies. No significant two-photon probe signal was observed.

8 Time-resolved Mass spectra

8.1 THP

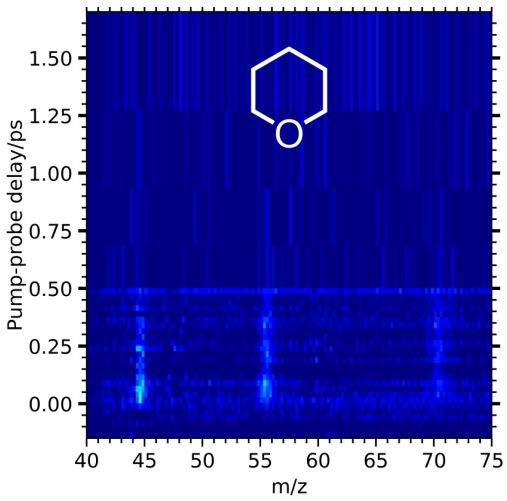

Figure 9: Time-resolved mass spectrum of THP.

8.2 THF

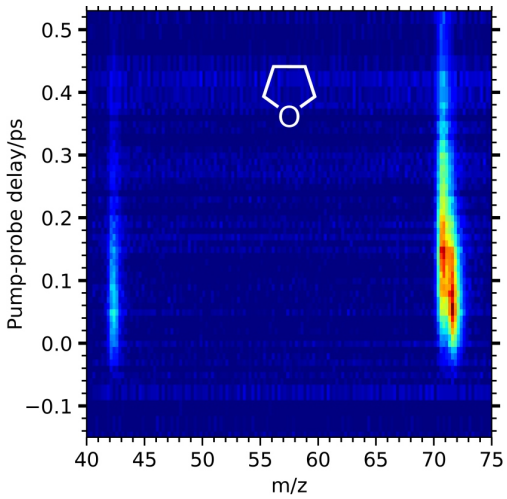

Figure 10: Time-resolved mass spectrum of THF.

8.3 TMO

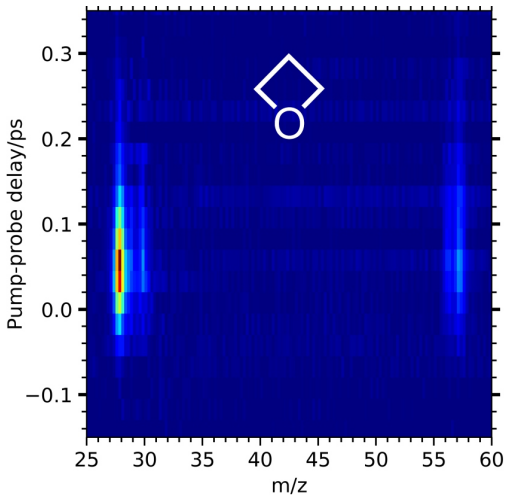

Figure 11: Time-resolved mass spectrum of TMO.

9 Photoelectron Angular Distributions

9.1 THP

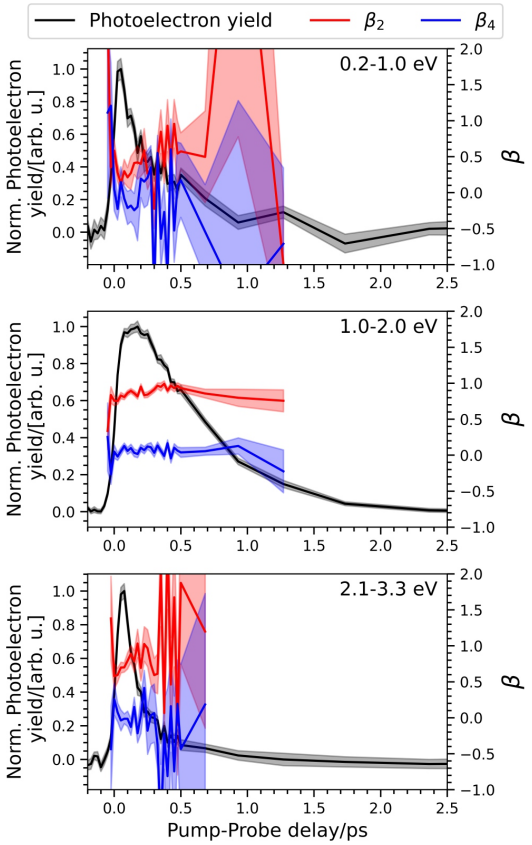

Figure 12: Decays and corresponding photoelectron anisotropy β_2 and β_4 of THP for different regions of interest, with error bars determined using a bootstrapping routine. If the total photoelectron intensity drops beyond 0.1 of the total photoelectron intensity, the signal-to-noise ratio is insufficient to fit the photoelectron angular distribution.

9.2 THF

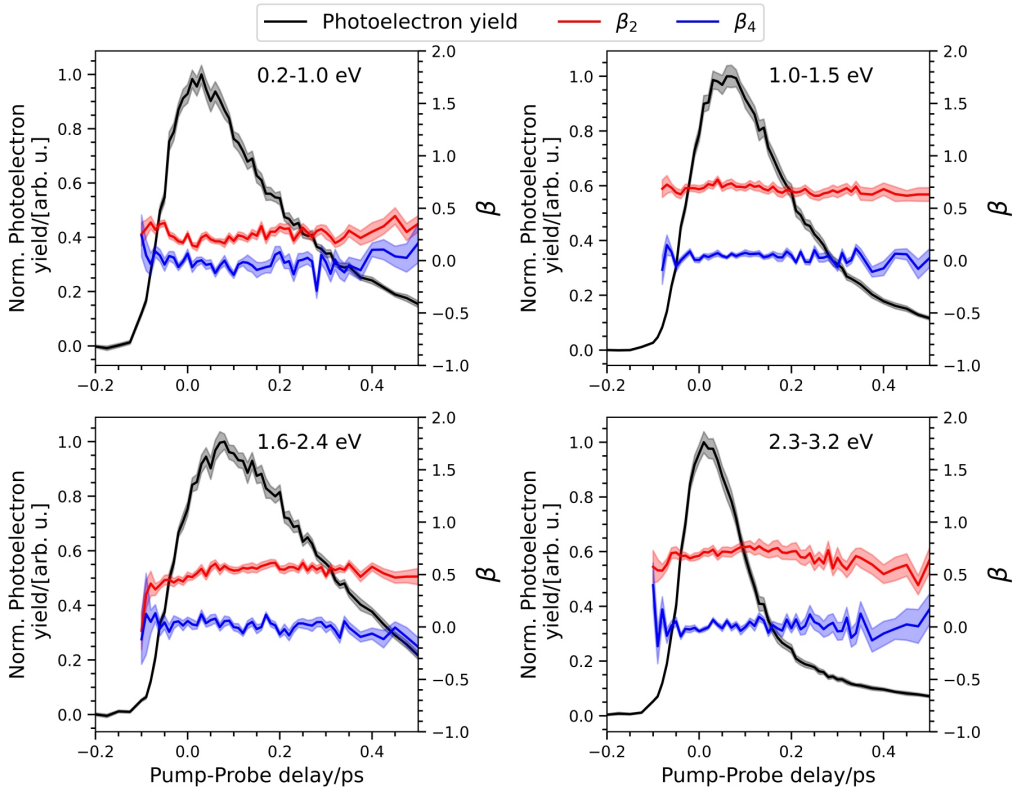

Figure 13: Decays and corresponding photoelectron anisotropy β_2 and β_4 of THF for different regions of interest, with error bars determined using a bootstrapping routine.

9.3 TMO

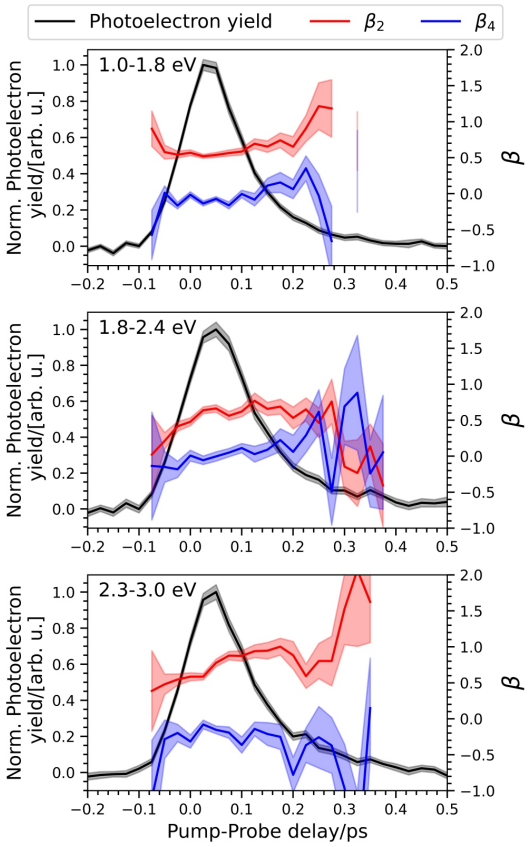

Figure 14: Decays and corresponding photoelectron anisotropy β_2 and β_4 of TMO for different regions of interest, with error bars determined using a bootstrapping routine.

10 Time-slices of the TRPES

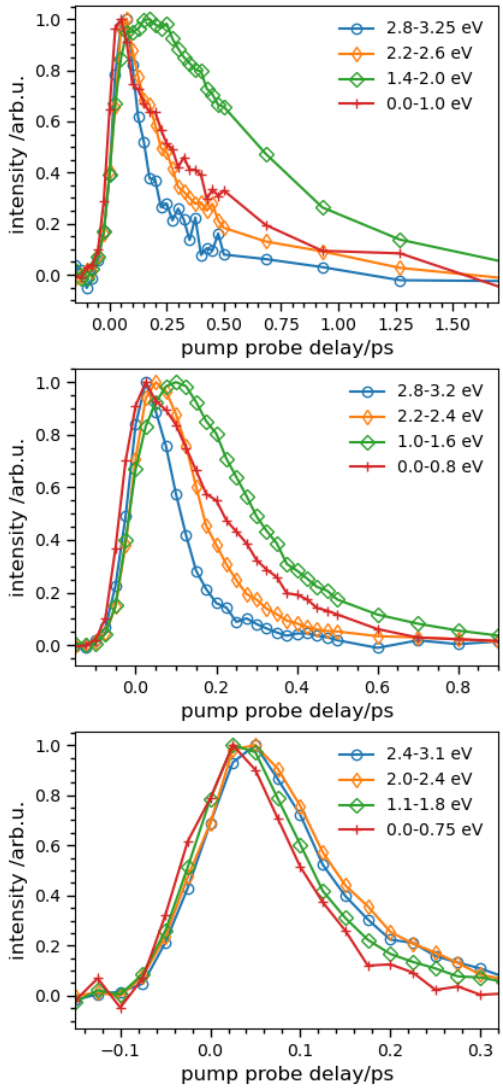

Figure 15: Temporal evolution for slices of the TRPES of THP (top), THF (middle) and TMO (bottom) in certain energy ranges.

11 Time-slices for TMO

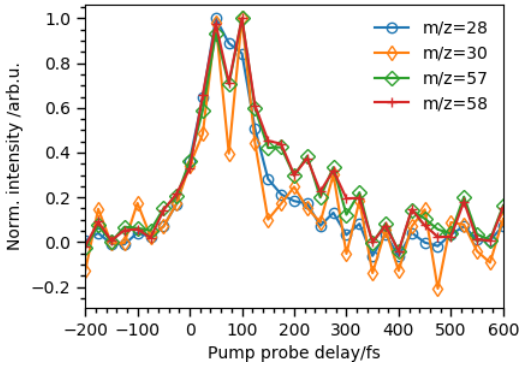

Figure 16: Temporal evolution for slices of the TRMS of TMOF for different masses.

12 Ringstrain

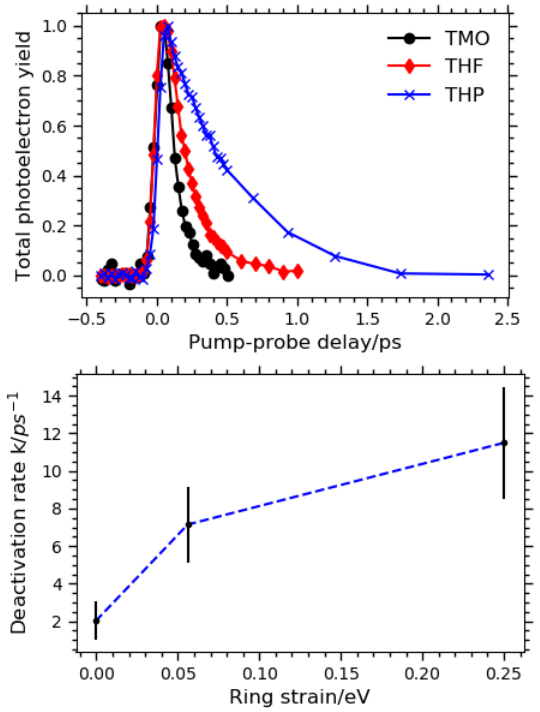

Figure 17: Top: Comparison of the decays of the total photoelectron yield of TMO, THP and THF. Bottom: Ring strain[1] versus deactivation speed for the three cyclic ethers.

13 Fitting functions

13.1 Mono-exponential fit

A mono-exponential decay of the form $A \xrightarrow{\tau_1} B$, where only A gives a measurable signal, is described by the differential equation

$$\lambda_1[A] = -\frac{d[A]}{dt}$$

λ_1 is the exponential decay constant ($\tau_1 = \frac{1}{\lambda_1}$). Solving this equation leads to

$$A(t) = A_0 e^{-\lambda_1 t}$$

where A_0 corresponds to the concentration of A at t=0. Both lasers (pump-probe) have a finite time y(t) where they interact with the sample

$$y(t) = Be^{-\frac{t^2}{2\sigma^2}}$$

where B is a scaling factor, and σ is related to the full-width-at-half-maximum of the laser via $fwhm = 2\sqrt{2ln2}\sigma$. The evolution of the detectable signal S(t) is obtained by convoluting A(t) and y(t), leading after simplification to

$$S(t) = \sigma_1 e^{\frac{\sigma^2}{2}\lambda_1^2 - \lambda_1 t} erfc(\frac{-t + \sigma^2\lambda_1}{\sqrt{2}\sigma})$$

σ_1 corresponds to a scaling factor, erfc is the complementary error function. The TRPES and TRMS of TMO are fitted using this equation in a global fitting approach: for each decay trace at a a given photoelectron energy or m/z ratio, a σ_1 is determined (corresponding to the the decay-associated spectrum at the given photoelectron energy or m/z ratio), wheras λ_1 (τ_1) is fitted globally to all decay traces. The fwhm of the laser was determined as described in the experimental section.

13.2 Bi-exponential sequential fit

A sequential bi-exponetial decay $A \xrightarrow{\tau_1} B \xrightarrow{\tau_2} C$, where both A and B give a measurable signal, can be described by two differential equations:

$$\frac{d[A]}{dt} = -\lambda_1[A]$$

$$\frac{d[B]}{dt} = \lambda_1[A] - \lambda_2[B]$$

$\lambda_{1,2}$ are the exponential decay constants($\tau_{1,2} = \frac{1}{\lambda_{1,2}}$). Solving these differential equations, results in:

$$A(t) = A_0 e^{-\lambda_1 t}$$

$$B(t) = \frac{\lambda_1}{\lambda_2 - \lambda_1} A_0 (e^{-\lambda_1 t} - e^{-\lambda_2 t})$$

The total signal is then the sum of A(t) and B(t) convoluted with the laser response y(t), resulting in

$$\begin{aligned} S(t) =& \sigma_1 e^{(\frac{\sigma^2}{2}\lambda_1^2 - \lambda_1 t)} erfc(\frac{-t + \sigma^2\lambda_1}{\sqrt{2}\sigma}) + \\ & \sigma_2 \frac{\lambda_1}{\lambda_2 - \lambda_1} (e^{(\frac{\sigma^2}{2}\lambda_1^2 - \lambda_1 t)} erfc(\frac{-t + \sigma^2\lambda_1}{\sqrt{2}\sigma}) - e^{(\frac{\sigma^2}{2}\lambda_2^2 - \lambda_2 t)} erfc(\frac{-t + \sigma^2\lambda_2}{\sqrt{2}\sigma})) \end{aligned}$$

The TRPES and TRMS of THF and THP are fitted using this equation analogous to the previous section.

	THF (C_S)				TMO (C_{2v})			
	Sym.	E/eV (nm)	$f/10^{-4}$	Character	Sym.	E/eV (nm)	$f/10^{-4}$	Character
1	2A'	6.57 (189)	153	n-Ry3s	$1B_2$	6.29 (197)	28	n-Ry3s
2	3A'	7.14 (174)	653	n-Ry3p_y	$2B_2$	6.65 (186)	128	n-Ry3p_x
3	1A"	7.27 (171)	37	n-Ry3p_z	$1A_2$	6.85 (181)	0	n-Ry3p_z
4	4A'	7.41 (167)	106	n-Ry3p_x	$2A_1$	7.01 (177)	6	n-Ry3p_y
5	**5A'**	**7.83 (158)**	**76**	**n-Ry3d_{z^2}**	**$3B_2$**	**7.71 (161)**	**153**	**n-Ry3d_{z^2}**
6	2A"	8.05 (154)	38	n-Ry3d_{xz}	**$3A_1$**	**7.98 (155)**	**305**	**n-Ry3d_{xz}**
7	3A"	8.17 (152)	98	n-Ry3d_{zy}	$1B_1$	7.99 (155)	808	σ-Ry3s
8	6A'	8.18 (152)	98	n-Ry3d_{xy}	$2A_2$	8.24 (151)	0	n-Ry3d_{xy}
9	7A'	8.47 (146)	89	n-Ry3$d_{x^2-y^2}$	$4A_1$	8.36 (148)	38	n-Ry3d_{zy}

Table 9: The symmetries and vertical excitation energies E of first nine excited states of THF and TMO calculated at the ADC(2.5)/aug-cc-pVDZ level of theory with the corresponding oscillator strengths f calculated at the ADC(3)/aug-cc-pVDZ level of theory. The electronic states relevant to the present experiments are marked in bold.

14 Excited states of C_S-symmetric THF and C_{2v}-symmetric TMO

15 The C_2-conformer as the the dominant contributor to our excited state TRPES signal

There is an ongoing debate for THF as to whether the C_2 or C_S symmetry ground state is more stable[2–10]. The energy difference depends on the electronic structure method and basis set used[2,9], ranging[2–10] between 34 to 104 cm^{-1}, and, depending on the basis set, the C_S might be an inflection point (transition state) rather than a true minimum[9]. Recent b3lyp/aug-cc-pVDZ investigations of the ground state potential energy surface reveal that not only is energy difference between C_2 and C_S conformer small (37 cm^{-1}), but the barrier separating the two conformers is also low (57 cm^{-1})[10]. All methods agree that both the energy difference and the barrier between them are small (although there remains a controversy as to which conformer is more stable). Both the C_S and C_2 ground conformers of THF likely exist in our molecular beam, with the C_2 conformer being thermodynamically favoured. For the case of the THF cation, there is no controversy regarding the C_2 geometry of its ground state. Kwon et al. determined that the C_2 conformer is the true global minimum in the THF cation, whereas the C_S geometry is a saddle point on a steep part of cation potential energy surface[10]. Based on all evidence (as discussed in the main body of the text), the n=3 Rydberg states have geometries quite similar to that of the ground state cation. Therefore, we expect that the n=3 Rydberg states investigated here will likewise have the C_2 conformer geometry. In other words, we do not expect that there exist n=3 Rydberg states of C_S conformer symmetry. For a given conformer to

contribute to our TRPES signal, the conformer must have a sufficiently high absorption cross section at our VUV pump laser wavelength to be excited. In our experiments, we excited into the 3d Rydberg manifold with a fixed pump photon energy of 7.75 eV. We assume that the 3d Rydberg states have C_2-symmetry geometries and that their potential energy surfaces are likely parallel: such Rydberg states are 'nested potentials'. In the cation ground state and the 3d Rydberg states, the C_S geometry is but a point of inflection on a steep part of their respective potential energy surfaces. Therefore, excitation from a ground state C_S conformer into a C_2-geometry 3d Rydberg state corresponds to a transition into a vibrationally excited C_2 conformer 3d Rydberg state. This situation is depicted in SI Fig. 18 below. In our TRPES experiments, the pump photon energy is fixed at 7.75 eV. Starting from the ground state C_2 conformer, we will excite mainly into the $3d_{yz}$ Rydberg state (oscillator strength of 640 x 10^{-4} and vertical excitation energy of 7.82 eV, see Table 1 in the main paper) with negligible vibrational excitation. In contrast, the ground state C_S conformer cannot be excited into the $3d_{yz}$ Rydberg state, as the pump photon energy cannot access the higher vibrationally excited C_2-geometries. These vibrationally excited geometries, however, are accessible in the next lower-lying 3d Rydberg state, $3d_{z^2}$ (see SI, Table 9). Importantly, we note that the $3d_{z^2}$ oscillator strength is 76 x 10^{-4}, about 8 times smaller than that of the $3d_{yz}$ Rydberg state. This strongly suggests that the ground state C_2 conformer in THF will predominantly contribute to transitions to the excited state. Therefore, we analyzed our TRPES data assuming that only the C_2 conformer contributes significantly to our excited-state signals.

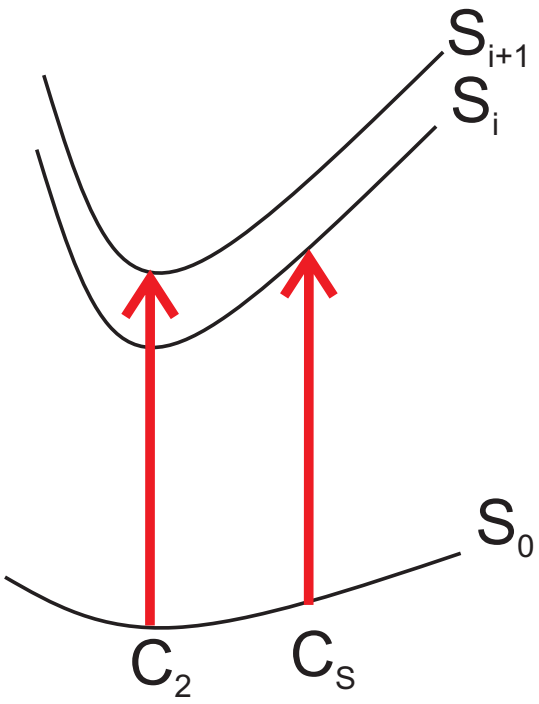

Figure 18: A cartoon depiction of pump transitions for the ground state conformers of THF. The potential energy surface on the S_0 ground state is shallow and the energy difference between the C_2 and C_S conformers is small (the barrier between these is not shown). S_i and S_{i+1}, represent the nested 3d Rydberg states which each have C_2 geometries similar to that of the cation. The red arrow symbolizes our fixed pump photon energy. The minimum energy C_2 conformer can be excited into the S_{i+1} Rydberg state. However, the C_S conformer, due to its distorted geometry, must make a transition into higher lying vibrational states of S_{i+1}. Since the pump photon energy is fixed at 7.75 eV, these higher lying vibrational states of S_{i+1} are inaccessible. Therefore, the fixed pump photon can only access higher lying vibrational states of the next lower 3d Rydberg state, S_i.

References

[1] T. Dudev and C. Lim, *J. Am. Chem. Soc.*, 1998, **120**, 4450–4458.

[2] A. Giuliani, P. Limao-Vieira, D. Duflot, A. R. Milosavljevic, B. P. Marinkovic, S. V. Hoffmann, N. Mason, J. Delwiche and M. J. Hubin-Franskin, *Eur. Phys. J. D*, 2009, **51**, 97–108.

[3] P. A. Baron and D. O. Harris, *J. Mol. Spectrosc.*, 1974, **49**, 70–81.

[4] R. Meyer, J. C. López, J. L. Alonso, S. Melandri, P. G. Favero and W. Caminati, *J. Chem. Phys.*, 1999, **111**, 7871–7880.

[5] A. H. Mamleev, L. N. Gunderova, R. V. Galeev and C. Physics, *J. Struct. Chem.*, 2001, **42**, 365–370.

[6] D. G. Melnik, S. Gopalakrishnan, T. A. Miller and F. C. De Lucia, *J. Chem. Phys.*, 2003, **118**, 3589–3599.

[7] B. Cadioli, E. Gallinella, C. Coulombeau, H. Jobic and G. Berthier, *J. Phys. Chem.*, 1993, **97**, 7844–7856.

[8] S. J. Han and Y. K. Kang, *J. Mol. Struct. THEOCHEM*, 1996, **369**, 157–165.

[9] V. M. Rayón and J. A. Sordo, *J. Chem. Phys.*, 2005, **122**, 204303.

[10] S. M. Park, Y. R. Lee, D. W. Kang, H. L. Kim and C. H. Kwon, *Physical Chemistry Chemical Physics*, 2017, **19**, 30362–30369.